Contrib. Mineral. Petrol. 65, 255–267 (1978)

Contributions to Mineralogy and Petrology

The Geochemical Origin of Sepiolite and Kerolite at Amboseli, Kenya

Ronald K. Stoessell* and Richard L. Hay
Department of Geology and Geophysics, University of California Berkeley, California 94720, U.S.A.

Abstract. A massive white sepiolite deposit at Amboseli precipitated from magnesium and silica released during the ground water dolomitization of an earlier lacustrine sepiolite. Kerolite has since formed in proximity to the massive sepiolite as an alteration product of sepiolite and as a ground water precipitate when the pH is below 8. Authigenic sepiolite also occurs in the overlying younger sediments. Kerolite is likely to occur but has not yet been positively identified.

Presently, ground waters within the Amboseli Basin are supersaturated with respect to sepiolite and kerolite. This supersaturation results from the weathering of alkaline olivine basalts on the edge of the basin. The precipitation of sepiolite and/or kerolite does not control ground water compositions in the basin. These reactions are slow compared to other aqueous-mineral reactions such as those maintaining carbonate mineral equilibria. Equilibrium between disordered-dolomite and calcite buffers the log $a_{Mg2+}/(a_{H+})^2$ as a function of log f_{CO_2} in ground waters in the proximity of the massive sepiolite. This reaction can help explain the presence of sepiolite associated with dolomites in other near-surface deposits besides Amboseli.

Introduction

Sepiolite, $Mg_2Si_3O_{7.5}(OH)\cdot 3H_2O$, is the most common magnesium silicate forming under earth-surface conditions. This study began as part of a laboratory and field investigation of the limiting geochemical restraints on sepiolite formation. Amboseli Basin was picked for the geochemical study, because the basin contains a massive, low temperature sepiolite deposit associated with dolomite in playa sediments (Sampson, 1966; Williams, 1972). This is a common low temperature sepiolite assemblage (Rogers et al., 1956; Parry and Reeves, 1968; Papke, 1972).

During the course of the investigation, kerolite, $Mg_3Si_4O_{10}(OH)_2\cdot nH_2O$, was identified as a major mineral constituent of the massive sepiolite deposit at Amboseli. Kerolite is an uncommon, hydrous, talc-like mineral formerly thought to be a mixture of stevensite and serpentine (Brindley et al., 1977). The field occurrences of kerolite are not well documented. Maksimović (1966) has described kerolite from Goleš Mountain, Yugoslavia, associated with a nickel deposit in a laterite, and kerolite similar to Amboseli kerolite has been reported from Carter's Mine, Madison County, North Carolina (David Bish, personal communication, 1977). At Amboseli, kerolite occurs in pockets and veins within massive dolomite and massive green sepiolite. Field relationships often suggest kerolite formed by the alteration of sepiolite.

This investigation answers the following questions concerning the formation of sepiolite and kerolite within the Amboseli Basin. What was the geochemical environment of formation of the massive sepiolite deposit, and what chemical conditions were necessary to alter sepiolite to kerolite? What is the distribution of sepiolite and kerolite in the younger sediments, and what was the geochemical depositional environment of these sediments? Does the weathering of alkaline olivine basalts in the basin produce ground waters saturated with respect to sepiolite and kerolite? Is the precipitation of sepiolite and kerolite rapid enough to maintain equilibrium with the associated ground waters? What other aqueous-mineral reactions promote the formation of sepiolite and kerolite?

Physiography, Climate, and Regional Geology

Amboseli Basin is a semiarid basin covering 400 square km on the Kenya-Tanzania border (Fig. 1). Williams (1972) described the physiography, climate, and regional geology. The basin is a nearly

* Present address: Exxon Production Research Company, P.O. Box 2189, Houston, Texas 77001, U.S.A.

0010-7999/78/0065/0255/$2.60

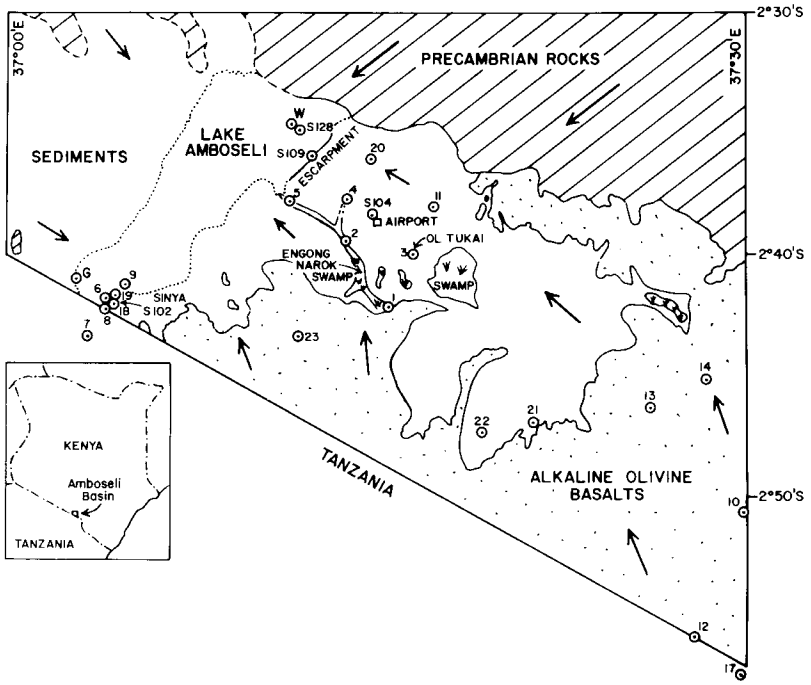

Fig. 1. Sketch map of Amboseli Basin (drawn from the geologic map of Amboseli Basin, Williams (1972)). The numbers refer to locations of mineral and water samples listed in Tables 1 and 3, respectively. The regional surface and ground water flow pattern is indicated by arrows

flat plain with an average elevation of 1140 m. The eastern half contains several spring-fed swamps, and the western half is dominated by a 21-km-long lake bed, Lake Amboseli, which bears water only during the brief rainy seasons. The basin is bounded on the north by low hills rising in elevation to between 1250 and 1400 m. Mt. Kilimanjaro dominates the southern edge of the basin, reaching an elevation of nearly 6000 m.

Rainfall within the basin is limited to between 25 and 50 cm per year. The major ground water sources lie to the south on the northern slopes of Mt. Kilimanjaro. Melted snow and rain water, from these slopes, flow northward into Amboseli Basin as streams and ground water. The streams dry up near the foothills of Mt. Kilimanjaro. The regional flow pattern of ground and surface waters are indicated by arrows on Figure 1.

The hills forming the northern boundary of Amboseli Basin are composed of metamorphosed Precambrian sediments. These rocks are predominantly marbles but include gneisses, granulites, and schists. Precambrian granitoid gneisses occur on the western edge of the basin near the Kenya-Tanzania border. The southern and eastern margins of Amboseli Basin are formed by the Pleistocene alkaline olivine basalts of Kilimanjaro. Several small parasitic volcanic cones occur within the southcentral portion of the basin, separated by sediments from the main volcanic flows.

Amboseli Basin is filled with sediments of probable Pleistocene age which locally have a thin superficial cover of Holocene sediments. The Pleistocene sediments have a maximum thickness of 90 m under the dry lake bed; however, the thickness is usually much less. The sediments overlie Precambrian rocks on the northern and western portions of the basin and overlie and presumably interfinger with Pleistocene basalts on the southern and eastern portions.

Stratigraphy and Mineralogy of the Pleistocene Sediments

The Pleistocene sediments are called the Amboseli Lake Beds. They have been stratigraphically subdivided by Williams (1972) into three formations: the Sinya Beds (the oldest formation), the Amboseli Clays, and the 01 Tukai Beds (the youngest formation). The three rock units are schematically illustrated in Figure 2.

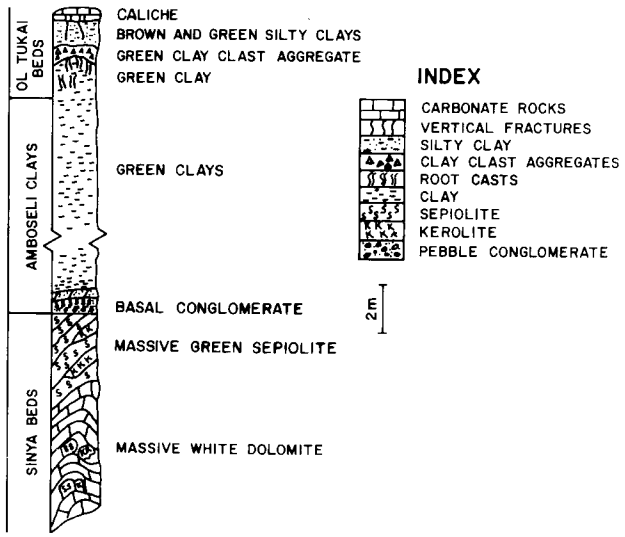

Fig. 2. Schematic representation of the exposed Pleistocene sediments in Amboseli Basin, beginning with the upper Sinya Beds and ending with the lower 01 Tukai Beds

The Sinya Beds are best exposed at the type locality at Sinya in Kenya (Fig. 1). An 8-m thickness of the Sinya Beds has been exposed by sepiolite mining operations along the axis of a small dome. The beds have been folded, fractured, and are separated by an angular unconformity from the overlying Amboseli Clays. The exposed section of Sinya Beds consists of 5 m of hard, massive white dolomite conformably overlain by 3 m of hard, massive, green sepiolite. The contact between the dolomite and green sepiolite is generally sharp.

Pockets and veins of massive, white sepiolite and pastel kerolites are scattered throughout the dolomite and the green sepiolite. These minerals generally have a sharp contact with the host rocks. The kerolites occur as fine-grained waxy clays, having good conchoidal fracture and a tendency to break by spalling. The white sepiolite is characterized by a porous, chalky texture and a very low specific gravity. It is a very pure mineral and is easily distinguished from the green sepiolite on the basis of color, texture, lack of carbonate impurities, and stratigraphic relations. Typical X-ray diffraction patterns of the white sepiolite and the kerolites are given in Figure 3, and wet chemical analyses are listed in Table 1. The X-ray diffraction patterns of the kerolites often show minor amounts of a 7 Å phase (serpentine?) and an expandable smectite (stevensite?).

The white sepiolite often forms the cores of small folds in the dolomite. Kerolite occasionally occurs around the sepiolite, separating it from the dolomite. X-ray diffraction patterns of the encompassing kerolite sometimes show the presence of a minor sepiolite component. The dolomite surface often has desiccation-type cracks which have sometimes been filled with white sepiolite (Fig. 4). From these field observations, we believe the white sepio-

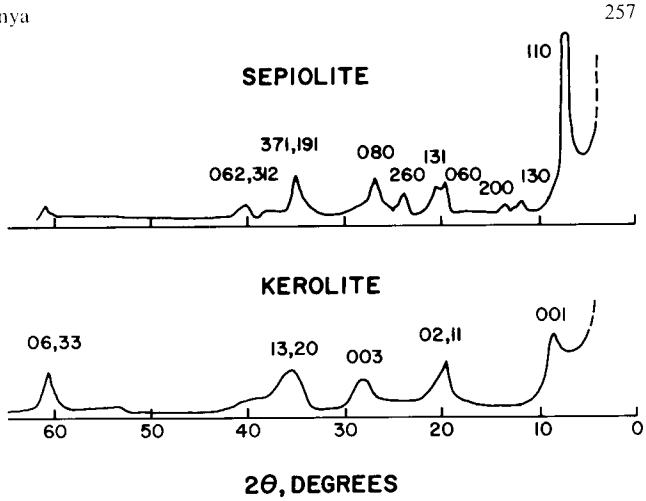

Fig. 3. Typical Co radiation X-ray diffraction patterns for Amboseli sepiolites and kerolites. The hkl values for sepiolite are from Brindley (1959), and the values for kerolite are from Brindley et al. (1977)

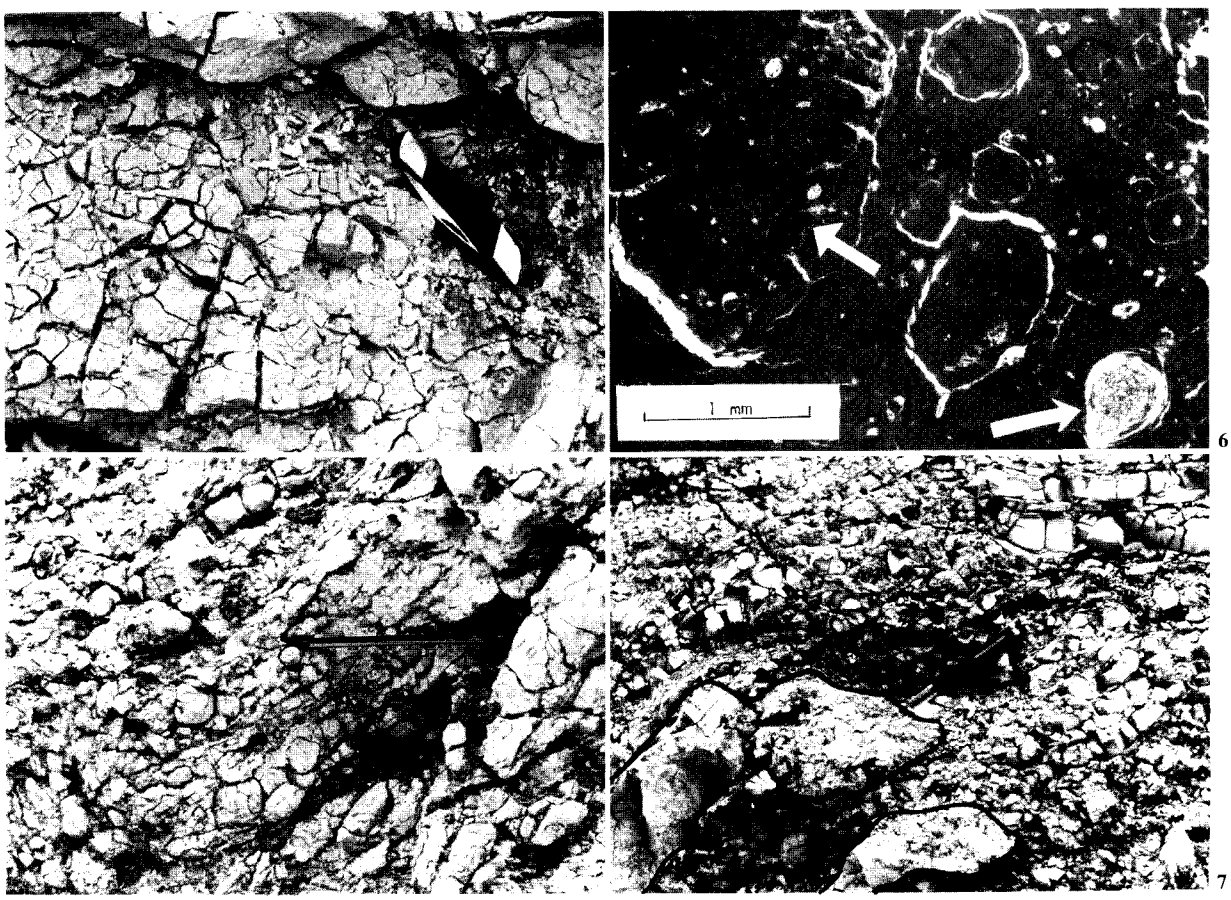

Fig. 4. Photograph of desiccation cracks in dolomite in the Sinya Beds. The white material filling some of the cracks is sepiolite

Fig. 5. Photograph of the weathered surface of the dolomite in the Sinya Beds, showing the nodular texture

Fig. 6. Photograph of a thin section under crossed-nicols of dolomite in the Sinya Beds. The matrix material is dolomite which has completely dolomitized some of the nodules. The residual light and dark minerals occupying the cores of some of the nodules (see arrows), are magnesium silicates of sepiolite composition. The rock has fractured around the nodules, and the cracks have been filled with white calcite

Fig. 7. Photograph of weathered, massive green sepiolite (see outlined areas) in the Sinya Beds. The sepiolite is surrounded by thin beds of kerolites showing their characteristic nodular fracture surfaces

lite and the kerolites formed after the dolomite, and that the kerolites may sometimes be an alteration product of sepiolite.

Nodules are often found weathering out of the surface of the dolomite (Fig. 5). The nodular texture of the dolomite also exists on a microscopic scale as illustrated by peloids in the thin section in Figure 6. Some of the cores of the nodules contain a magnesium silicate which microprobe analyses show to be compositionally equivalent to sepiolite. Calcite has filled microcracks and microveins within the dolomitic matrix. From these observations, we believe dolomitization of an earlier sepiolite has occurred, followed by later deposition of calcite. This earlier sepiolite does not correlate with the massive white sepiolite which formed later as a secondary deposit.

The green sepiolite, overlying the dolomite, contains numerous fine veins of white dolomite and calcite. These veins are visible in hand specimens. Upon weathering, the green sepiolite becomes friable and the carbonate content increases. The weathered green sepiolite is often surrounded by thin sheets of kerolite (Fig. 7). In such cases, the contact is sometimes graditional over a distance of 1 or 2 cm, grading from very weathered green sepiolite through a calcareous friable clay into kerolite. Alteration of sepiolite to kerolite may have caused these occurrences of kerolite surrounding sepiolite.

The Amboseli Clays are a sequence of friable, massive, lacustrine green clays which have a maximum thickness of 60 m under the dry lake bed of Lake Amboseli (Williams, 1972). The upper contact with the 01 Tukai Beds is obscured, but the lower contact, exposed at Sinya, is marked by a basal conglomerate overlying an angular unconformity. This investigation was limited to the exposures of the lower Amboseli Clays at Sinya, the exposures of the upper Amboseli Clays just beneath the lake bed surface, and two shallow cores taken from boreholes in the lake bed. The locations of the cores, G and W, are marked on Figure 1. Core samples were supplied by F.J. Matheson to R.L. Hay in 1964 for cores G and W to depths of 10 and 5 m, respectively.

The basal conglomerate is composed predominantly of dolomite and sepiolite clasts with a few fragments of kerolite. Sand matrix of the conglomerate includes a small percentage of metamorphic quartz, garnet, and oligoclase. A very few fragments of volcanic debris containing andesine in the sand fraction, are the oldest sedimentary evidence for the presence of the nearby alkaline olivine basalts.

The mineralogy of the fine-grained Amboseli Clays lying above the conglomerate is remarkably uniform. The assemblage is sepiolite, calcite, dolomite, a 10 Å clay, and K feldspar. In addition, gaylussite occurs near the lake bed surface over the southern half of Lake Amboseli. Sepiolite also fills thin veins in the lower Amboseli Clays (Fig. 8). These veins are usually parallel to bedding, but sometimes cut across bedding, indicating a secondary origin. The K feldspar is presumably authigenic, because it gives an X-ray diffraction pattern like that described by Martin (1971). The 10 Å spacing is broad, non-expandable, and does not collapse to 7 Å with heating to 200° C. Ordinarily, we would assume this to be an illite; however, kerolite has a somewhat similar 10 Å spacing. Kerolite shows a slight expansion after prolonged exposure to ethylene glycol (Brindley and others, 1977). Because the 10 Å clay is non-expandable, we believe it to be illite; however, the magnitude of the expansion for kerolite may not be observable if it is only a minor component.

The 01 Tukai Beds, the youngest formation of the Amboseli Lake Beds, are a sequence of silts, clays, clay-clast aggregates, and caliches. The formation has a maximum thickness of 25 m near the town of 01 Tukai (Williams, 1972). The lower 01 Tukai Beds crop out on an escarpment, 2 and $^1/_2$ m high, which forms the northeast edge of the dry lake. Outcrops of caliche form erosional remnants on the surface near the 01 Tukai Airport and also line a canal, the Simek Causeway (Fig. 1). The upper 01 Tukai Beds underlie the eolian and fluvial deposits of Holocene sediments covering the eastern half of the basin. These beds do not contain sepiolite or kerolite and are not further discussed in this report.

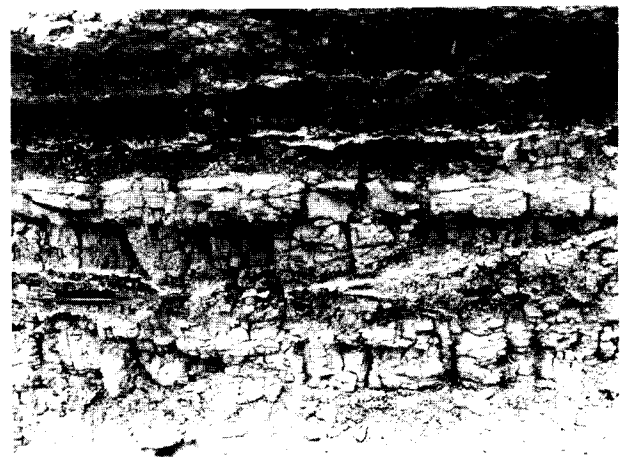

Fig. 8. Photograph of white veins of sepiolite (see knife), interbedded with green clays and white calcareous marls, in the lower Amboseli Clays. The massive white bed at the bottom of the picture is a sandstone lens which overlies the basal conglomerate (not shown) of the Amboseli Clays

The stratigraphic position of the contact with the underlying Amboseli Clays is unclear from the description given by Williams (1972). In this study, the basal bed of the 01 Tukai Beds was taken to be the lowest bed exposed on the escarpment along the lake shore. This bed is a green lacustrine clay similar in appearance to the underlying green lacustrine clays of the Amboseli Clays. This similarity prevented the differentiation of the contact between the Amboseli Clays and the 01 Tukai Beds.

The 2.5-m thickness of the lower 01 Tukai Beds, exposed on the escarpment, ranges from green lacustrine clays at the base to brown and green silty clays at the top. Locally, a green clay-clast aggregate separates the lacustrine clays from the silty clays. This aggregate bed covers a surface eroded on the lacustrine clay. The aggregates vary from silt to pebble-size and are probably of fluvial origin. The silty clay is predominantly composed of silt and clay-size aggregates, presumably of eolian origin.

The lower 01 Tukai Beds consist chiefly of the minerals sepiolite, analcime, calcite, a 10 Å clay, and minor amounts of K feldspar. Root casts are everywhere abundant in these beds and are usually filled with calcite. Some root casts in the silty clays are filled with a green mixture of sepiolite and opaline silica. The aggregates, in the silty clays and the clay clast aggregate bed, are composed of sepiolite and the 10 Å clay. Diatoms and phytoliths occur in the silty clays, and metamorphic and volcanic detritus together with bones and shells are locally abundant in the clay-clast aggregate.

The minerals in the clay-clast aggregate and the silty clays are of both detrital and authigenic origin. The Amboseli Clays and the basal bed of the 01 Tukai Beds are presumably the source beds for detrital sepiolite, the 10 Å clay, and K feldspar. Analcime is presumably authigenic in the basal bed and may be detrital above. Sepiolite, calcite, and opaline silica are authigenic when present as root cast fillings.

The silty clays of the lower 01 Tukai Beds grade upward into caliche, and the contact is particularly well-exposed along the Simek Causeway. The thickness of the caliche ranges from

2 m near the causeway to 1 m in the vicinity of the airport. The color varies from white to black but is usually brown. Soil fragments are common, and root casts are everywhere abundant. The caliche near the airport has been partially silicified, containing 25 wt. % SiO_2 (Table 1). The source of this silica was probably the phytoliths and diatoms found in the 01 Tukai Beds.

Bulk Chemical Compositions of the Pleistocene Sediments

Table 1 contains bulk wet chemical analyses, made in duplicate, on 12 samples selected from the Sinya Beds, Amboseli Clays, and the lower 01 Tukai Beds. These data were used to estimate an average chemical composition for each formation, and these estimates are given in Table 2. The significant chemical trends in Table 2 can be used to infer differences in the geological environments of deposition for the forma-

Table 1. Chemical analyses of Amboseli sediments[b]

	s.d.[a]	1[c]	2[c]	3	4	5	6
SiO_2	0.09	53.70	54.51	55.94	55.21	3.66	53.17
TiO_2	0.01	0.12	0.03	0.11	0.06	0.01	0.17
Al_2O_3	0.04	1.15	0.49	1.16	0.67	0.18	1.76
Fe_2O_3	0.02	0.64	0.10	0.72	0.10	0.09	0.99
FeO		0.02		0.02			0.04
MnO		0.00	0.00	0.01	0.00	0.00	0.01
NiO		0.000	0.000	0.006	0.002	0.005	0.000
MgO	0.05	23.31	28.01	26.50	27.14	20.11	24.70
CaO	0.02	0.03	0.52	0.25	0.56	31.48	0.23
Na_2O	0.02	0.67	0.85	0.56	1.00	0.06	0.45
K_2O	0.03	0.61	0.26	0.85	0.42	0.01	0.97
P_2O_5		0.02	0.03	0.03	0.01	0.06	0.04
$H_2O^+ + CO_2$		9.83	7.97	7.54	7.36	44.78	8.29
H_2O^-		9.76	7.18	6.53	7.17	0.38	8.79
Total		99.86	99.95	100.23	99.70	100.83	99.61

[a] Standard deviations were computed from duplicate analyses of major oxides on all samples

[b] R. Stoessell did the analyses using a modified procedure of Shapiro and Brannock (1962). Totals of H_2O^+ and CO_2 were computed using ignition loss with a correction for FeO

Samples 1, 2, 3, 4, 5, and 6 are from the Sinya Beds: 1, massive white sepiolite; 2, gray kerolite; 3, green kerolite; 4, white kerolite; 5, massive white dolomite; 6, massive green sepiolite

[c] Samples 1 and 2 represent the purest specimens collected of sepiolite and kerolite, respectively. The computed formula for the white sepiolite (sample 1), based on 8 oxygens to balance all cations except H^+, is $(Mg_{1.90}Na_{0.07}K_{0.04})$ $(Si_{2.94}Al_{0.08}Fe_{0.03})O_{7.5}(OH)_2 \cdot 3.07\,H_2O$. Similarly, the computed formula for the gray kerolite (sample 2), based on 11 oxygens, is $(Na_{0.12}K_{0.03}Ca_{0.04})$ $(Mg_{2.99})$ $(Si_{3.91}Al_{0.04}Fe_{0.01})O_{10}(OH)_2 \cdot 2.62\,H_2O$. Fe in the formulas refers to Fe^{+3}

Table 1. (Continued)

	7	8	9	10	11	12
SiO_2	47.65	41.00	39.25	47.10	55.90	25.47
TiO_2	0.11	0.64	0.56	0.14	0.07	0.00
Al_2O_3	2.53	4.86	4.60	10.89	5.32	0.49
Fe_2O_3	0.47	2.95	2.69	6.81	3.48	0.39
FeO	0.10	0.08	0.08	0.32	0.20	0.14
MnO	0.00	0.03	0.06	0.05	0.03	0.02
MgO	22.88	17.17	11.60	6.36	8.95	1.73
CaO	1.83	6.80	4.76	0.49	1.68	37.54
Na_2O	0.82	1.07	6.44	3.83	3.48	0.42
K_2O	0.61	2.48	4.72	5.75	3.64	0.18
P_2O_5	0.10	0.20	0.37	0.39	1.99	0.12
$H_2O^+ + CO_2$	11.19	13.75	12.45	6.40	8.04	31.17
H_2O^-	11.49	8.68	11.77	8.78	6.25	1.29
NaCl	–	0.16	0.00	0.38	0.18	0.00
SO_3	–	0.03	0.10	0.03	0.00	0.03
Total	99.78	99.90	99.45	98.32	99.21	98.99

Samples 7, 8, and 9 are from the Amboseli Clays: 7, secondary vein sepiolite; 8, green clay, lower Amboseli Clays; 9, green clay, upper Amboseli Clays. Samples 10, 11, and 12 are from the 01 Tukai Beds: 10, green clay, basal bed of 01 Tukai Beds; 11, silty brown clay, lower 01 Tukai Beds; 12, caliche near the 01 Tukai Airport.

The sample locations are marked on figure 1. The samples came from these 4 locations: samples 1–8, S102; sample 9, S128; samples 10 and 11, S109; sample 12, S104

Table 2. Average chemical compositions of Amboseli sediments[a]

	Sinya Beds	Amboseli Clays	Lower 01 Tukai Beds
SiO_2	23.4	40.1	51.8
TiO_2	0.1	0.6	0.1
Al_2O_3	0.8	4.7	8.1
Fe_2O_3	0.5	2.8	5.1
FeO	0.0	0.1	0.3
MnO	0.0	0.0	0.0
NiO	0.0	–	–
MgO	21.8	14.4	7.7
CaO	19.0	5.8	1.1
Na_2O	0.2	3.8	3.7
K_2O	0.4	3.6	4.7
P_2O_5	0.1	0.3	1.2
$H_2O^+ + CO_2$	30.2	13.1	7.2
H_2O^-	3.7	10.2	7.5
NaCl	–	0.1	0.3
SO_3	–	0.1	0.0
Total	100.2	99.7	98.8

[a] The average chemical compositions were estimated using two representative samples from Table 1 for each formation. The Sinya Beds' composition was based on 60% of sample 5 and 40% of sample 6. The average of samples 8 and 9 was used for the Amboseli Clays, and the average of samples 10 and 11 was used for the lower 01 Tukai Beds

tions. The chemistry should reflect the presence or absence of detrital igneous material from the nearby olivine basalts.

The wt. % of Al_2O_3 increases from 0.8 to 8.1, going from the estimates of the Sinya Beds to those of the lower 01 Tukai Beds. Similarly, the wt. % of Fe_2O_3 (total iron) increases from 0.5 to 5.4. The absence of appreciable iron and aluminum in the Sinya Beds could be due to their removal by aqueous solutions or to the lack of detrital input of basaltic material. Alkaline olivine basalts are within the vicinity of the Sinya Beds' outcrop at Sinya (Fig. 1). A lack of detrital basaltic material would imply the Sinya Beds predated the extrusion of the basalts.

Aqueous solutions could have leached iron and aluminum from the Sinya Beds. Aluminum is appreciably soluble at both high and low pH values (Stumm and Morgan, 1970, p. 398); however, sepiolite, a common authigenic mineral in the Sinya Beds, forms only in basic solutions (Siffert, 1962). Therefore, one possibility is the removal of aluminum by waters having a high pH.

Iron is soluble in aqueous solutions under reducing conditions combined with a low to slightly basic pH (Garrels and Christ, 1965, p. 195). These aqueous conditions for soluble iron and aluminum do not overlap. Presumably, the low Al_2O_3 and Fe_2O_3 content of the Sinya Beds is due to a lack of detrital basaltic material, implying the basalts are younger then the Sinya Beds.

Other trends in Table 2 involve elements which are generally soluble in aqueous solutions. These trends are not definitive, because the increase or decrease can be explained by detrital mineral input, the removal or introduction of the elements by the associated waters, and sometimes by biologic activity.

Water Chemistry

The water chemistry within Amboseli Basin was used to infer possible chemical reactions between minerals and the associated waters. Table 3 contains the chemical compositions of 23 water samples taken in August, 1975, from throughout the southern and central portions of the basin. These samples are from streams, springs, wells, swamps, and pits (Fig. 1). Sample locations 15 and 16 are not shown on Figure 1; however, their locations are given in Table 3. Water samples were not available from the arid northern portion of the basin.

The sampling procedure began with field measurements of pH and alkalinity. These were made using an Orion Model 407A pH meter, buffered (± 0.02 log units) at pH values of 4, 7, and 10. A liter of each sample was field-filtered through a 0.1 micron filter, and the filtrate was divided into two $^1/_2$ l aliquots which were stored in clean plastic bottles. One of the aliquots was acidified to a pH of 3 with reagent grade HNO_3. Five ml of the non-acidified aliquot were diluted 1 to 10 with de-ionized water for later SiO_2 analyses. Blanks of HNO_3 and de-ionized water were kept for later analyses. Ca^{2+} and Mg^{2+} were measured in the field using EDTA titrations (Brown et al., 1970).

The complete analyses with the exceptions of F^- and SO_4^{2-} were made between two and three months after collection. F^- and SO_4^{2-} were analyzed one year after collection. The acidified aliquot was used for measuring Ca^{2+}, Mg^{2+}, Na^+, and K^+, and Al^{3+}, and the non-acidified aliquot was used for Cl^-, F^-, and SO_4^{2-}. SiO_2 was determined on the diluted aliquot. The estimated accuracies of these analyses are given in Table 3.

Total Ca^{2+}, Mg^{2+}, Na^+, and K^+ concentrations were measured with atomic absorption using a Perkin-Elmer Model 303 spectrophotometer. One thousand ppm La^{3+} were used to overcome SiO_2 and Al^{3+} interference for Ca^{2+} and Mg^{2+} and to reduce ionization of Na^+. The disagreement between the values of Ca^{2+} and Mg^{2+} determined by AA and by field titrations was less than 5%. The AA values were used because of the subjectivity involved in picking the EDTA end-points. The method of standard additions was used for K^+ to overcome ionization effects caused by Na^+. Total Al^{3+} values were obtained with atomic absorption using a Perkin-Elmer Graphite Furnace HGA 2100 Model 360 spectrophotometer.

SiO_2 and Cl^- were analyzed by the well-known molybdate blue colorimetric method and the Mohr titration method, respectively. For Cl^- concentrations of less than 35 ppm, a Radiometer CNT 10 chloride titrator was substituted for the visual endpoint determination. F^- was measured using a SPADNS-zirconium lake colorimetric determination (Bellack and Schouboe, 1958), and SO_4^{2-} was analyzed by a barium sulfate turbidimetric procedure (Tabatabai, 1974). A Zeiss Model PMQ11 spectrophotometer was used in the colorimetric and turbidimetric determinations.

The reported values of aluminum represent maximum values for reactive aluminum in solution. The 0.1 micron field-filtration was sufficient to remove most of the particulate matter; however, colloidal material and some clay particles would be expected to pass through the filter. This would produce a negligible positive error in the measured concentrations of the major aqueous elements, but might cause a significant increase in reported concentrations of trace

Table 3. Amboseli water chemical analyses in ppm[a]

Sample	°C ±0.5	pH ±0.05	SiO_2 ±2%	Al^{3+} ±8%	Mg^{2+} ±2%	Ca^{2+} ±2%	Na^{+} ±2%	K^{+} ±3%	Cl^{-} ±5%	SO_4^{2-} ±8%	F^{-} ±8%	$HCO_3^{-}+CO_3^{2-}$ in meq. ±0.03	Charge Balance meq.
1	18	7.00	39.8	0.0034	4.10	5.75	17.6	7.40	2.2	1.2	0.33	1.36	+0.08
2	19	6.50	43.9	0.055	7.63	13.9	27.0	10.8	3.1	1.4	0.63	2.46	+0.10
3	22	7.70	105.0	0.0015	34.2	56.9	59.3	24.4	3.6	5.0	2.9	7.98	+0.24
4	17	8.80	51.3	0.029	11.2	26.8	50.2	13.0	3.5	16.1	1.0	3.99	+0.20
5	20	7.30	56.9	0.010	20.5	58.0	45.4	14.6	2.8	0.2	1.3	6.59	+0.02
6	23	8.15	56.5	0.0005	11.6	10.0	274.0	36.1	205.0	21.6	1.4	8.28	−0.39
7	20	9.95	44.5	0.024	0.37	1.79	946.0	84.0	533.0	50.2	4.1	27.58	−0.42
8	22	8.30	63.3	0.0056	11.7	11.9	93.8	6.66	14.7	7.0	0.65	4.83	+0.24
9	25	9.85	43.4	0.067	0.31	8.10	2030.0	34.6	953.0	136.0	10.0	59.90	−0.46
10	18	7.95	49.6	0.0071	11.2	13.6	33.7	8.10	3.2	2.5	0.74	3.00	0.00
11	25	7.90	105.0	0.0005	16.6	17.3	741.0	92.6	73.0	360.0	5.8	27.04	−0.21
12	11	7.85	18.1	0.016	0.64	1.31	7.31	2.00	0.3	0.5	0.25	0.44	0.00
13	19	7.95	62.6	0.0091	15.1	22.2	25.1	5.70	2.3	2.4	0.34	3.31	+0.02
14	20	6.95	56.5	0.0007	11.6	15.8	21.6	7.25	2.6	2.0	0.30	2.59	+0.05
15	11	7.70	16.7	0.016	0.53	1.21	7.31	1.56	0.2	0.6	0.10	0.44	0.01
16	11	7.80	10.7	0.0092	0.43	0.90	4.80	1.30	0.2	0.5	< 10	0.33	−0.03
17	13	6.85	16.7	0.020	0.63	1.40	8.28	1.82	1.3	0.9	0.13	0.49	−0.04
18	23	7.90	94.4	0.0031	28.8	22.80	84.5	13.1	39.6	15.8	0.70	5.65	+0.14
19	22	9.90	27.0	0.034	1.52	2.80	391.0	44.6	155.0	20.1	2.8	13.78	−0.30
20	26	7.80	107.0	0.024	60.4	21.9	1010.0	114.0	127.0	580.0	3.5	36.53	+0.20
21	27	8.25	45.8	0.020	12.1	7.40	60.9	12.0	4.5	4.0	1.8	3.79	+0.12
22	21	7.20	49.6	0.0087	9.15	13.3	18.5	6.50	2.4	4.0	0.39	2.21	−0.07
23	20	7.10	38.1	0.0110	7.33	10.8	8.82	2.52	1.4	1.8	0.14	1.46	0.00

Sample locations: 1. Serena Lodge Spring in basalt. 2. Engong Narok Swamp in Holocene sediments. 3. 01 Tukai well in 01 Tukai Beds, w.l. = −8 m. 4. Kioko's Ditch (swamp) in 01 Tukai Beds. 5. Simek Causeway (swamp) in 01 Tukai Beds. 6. Sinya well in dolomite, w.l. = −3 m. 7. Sinya (Tanzania) meerschaum pit in dolomite. 8. Sinya Masai well in dolomite, w.l. = −3 m. 9. Gaylussite pit in Amboseli Clays. 10. Kimengelia Stream in basalt conglomerate at the East Gate of Amboseli Park. 11. Borehole C3045 in 01 Tukai Beds, w.l. = −12 m. 12. Kimengelia Stream in basalt on the Kenya-Tanzania border. 13. Lemongo Spring in basalt. 14. Legumi Spring in basalt. 15. Kimengelia Stream in basalt at 2680 m elevation. 16. Nalemoru Stream in basalt at 2680 m elevation. 17. Nalemoru Stream in basalt at 1890 m elevation (low pH and abnormal Cl content indicate ground water). 18. Sinya spring in dolomite. 19. Sinya meerschaum pit in dolomite. 20. Borehole C2839 in 01 Tukai Beds, w.l. = −9 m. 21. Borehole C2794 in basalt, w.l. = −177 m. 22. Borehole C3046 in basalt, w.l. = −110 m. 23. Borehole C3043 in basalt, w.l. = −27 m

[a] The samples were collected in August, 1975, at the locations marked on Figure 1. The ± values refer to estimated accuracies using the analytical procedures described in the text

elements. Aluminum is a trace element because it occurs in the parts-per-billion range.

The analytical data presented in Table 3 need to be converted to activities to make thermodynamic calculations. The activities were obtained by distributing the measured total element concentrations among the known aqueous species assuming thermodynamic equilibrium. In this calculation, the extended Debye-Hückel equation (Helgeson, 1969) was used in the calculation of activity coefficients. Table 4 lists the 25° C aqueous dissociation constants used in this study. The water samples were taken at temperatures ranging from 11° to 27°; however, most of the samples were within 5° of 25° C. The temperature dependence of the dissociation constants was found to produce negligible changes in the computed activities of the major cations and anions, but to produce significant differences (up to 0.5 log units) in the case of Al^{3+}. The constants listed in Table 4 were adjusted by a linear extrapolation of the relative temperature dependence of the constants listed at 0°, 25° and 50° by Kharaka and Barnes (1973) in *Solmneq*.

The actual computation of the activities for each sample was done with *Solveq*, a computer program written by Reed (1977). *Solveq* works by setting up, in terms of basic thermodynamic components, a series of equations for the dissociation reactions, mass balance relations, and electrical neutrality. The equations are then solved simultaneously using a Newton-Raphson iteration procedure.

The primary surface and ground water flow into the basin begins on the northern slopes of Kilimanjaro and ends under the dry lake bed of Lake Amboseli. The general flow pattern is shown on Figure 1. The water samples in this study were taken from the lower slopes of Kilimanjaro to the eastern and southern

Table 4. Aqueous thermodynamic dissociation constants at 25° C and 1 bar[a]

Reaction	Log K	Source
$OH^- + H^+ = H_2O$	14.00	1
$HCl = H^+ + Cl^-$	6.10	1
$CO_{2(gas)} + H_2O = 2H^+ + CO_3^{2-}$	−18.16	1
$HCO_3^- = H^+ + CO_3^{2-}$	−10.33	1
$H_2CO_3 = 2H^+ + CO_3^{2-}$	−16.67	1
$HF = H^+ + F^-$	− 3.18	1
$HSO_4^- = H^+ + SO_4^{2-}$	− 1.99	1
$H_3SiO_4^- + H^+ = 2H_2O + SiO_2$	9.65	1
$NaCl = Na^+ + Cl^-$	0.90	1
$NaHCO_3 = Na^+ + H^+ + CO_3^{2-}$	−10.08	2
$NaCO_3^- = Na^+ + CO_3^{2-}$	− 1.27	1
$Na_2CO_3 = 2Na^+ + CO_3^{2-}$	0.68	2
$NaSO_4^- = Na^+ + SO_4^{2-}$	− 1.17	1
$KCl = K^+ + Cl^-$	1.35	1
$KHSO_4 = K^+ + H^+ + SO_4^{2-}$	− 2.26	1
$KSO_4^- = K^+ + SO_4^{2-}$	− 0.85	1
$CaOH^+ + H^+ = Ca^{2+} + H_2O$	12.62	1
$CaHCO_3^+ = Ca^{2+} + H^+ + CO_3^{2-}$	−11.58	1
$CaCO_3 = Ca^{2+} + CO_3^{2-}$	− 3.20	1
$CaSO_4 = Ca^{2+} + SO_4^{2-}$	− 2.31	1
$Mg(OH)^+ + H^+ = Mg^{2+} + H_2O$	11.80	1
$MgHCO_3^+ = Mg^{2+} + H^+ + CO_3^{2-}$	−11.22	1
$MgCO_3 = Mg^{2+} + CO_3^{2-}$	− 2.99	3
$MgF^+ = Mg^{2+} + F^-$	− 1.82	2
$MgSO_4 = Mg^{2+} + SO_4^{2-}$	− 2.40	1
$Al(OH)^{2+} + H^+ = Al^{3+} + H_2O$	4.75	1
$Al(OH)_2^+ + 2H^+ = Al^{3+} + 2H_2O$	9.01	1
$Al(OH)_4^- + 4H^+ = Al^{3+} + 4H_2O$	23.27	1
$AlF^{2+} = Al^{3+} + F^-$	− 6.97	2
$AlF_2^+ = Al^{3+} + 2F^-$	−12.60	2
$AlF_3 = Al^{3+} + 3F^-$	−16.65	2
$AlF_4^- = Al^{3+} + 4F^-$	−19.04	2
$AlSO_4^+ = Al^{3+} + SO_4^{2-}$	− 3.05	1
$Al(SO_4)_2^- = Al^{3+} + 2SO_4^{2-}$	− 4.95	1

1 = Reed (1977); 2 = Kharaka and Barnes (1973); 3 = Siebert (1974)

[a] With the exception of Siebert (1974), the dissociation constants were taken from literature compilations used in *Solveq* and *Solmneq*, aqueous species distribution programs written by Reed and Kharaka, respectively

edges of the dry lake bed. No samples were available of ground waters beneath the lake bed; however, Williams (1972) lists several partial chemical analyses of waters taken from lake bed boreholes. These waters are predominantly CO_3^{2-} and HCO_3^- brines. Cation analyses were not reported.

Weathering and precipitation reactions of silicates produce a 1:1 equivalency between changes in cation concentrations and changes in alkalinity (Garrels, 1967; Berner, 1971, p. 175). At Amboseli, alkalinity and total cation concentrations are equivalent for most samples having alkalinity values less than 8 meq. ($10^{0.9}$ meq.). This is shown in Figure 9. The chemistry of these samples is predominantly due to weathering and precipitation reactions. Samples containing more than 8 meq. of alkalinity have appreciable chloride and sulfate concentrations. These anions either originated from the dissolution of soluble chlorides and sulfates or resulted from mixing with more saline waters, such as the brines underlying the dry lake bed.

The swamp water samples (2, 4, and 5) are not included in the following discussions. Their high organic content introduces unknown complexing effects, making it impossible to correctly calculate mineral log activity solubility products.

The water samples do not show a continuous increase in the activity solubility products of the carbonate minerals as the alkalinities increase. Figures 10 and 11 show the calcite and dolomite log activity solubility products for the water samples, plotted versus log meq. of alkalinity. The calcite and disordered-dolomite saturation lines were computed from data given by Helgeson et al. (1977). Disordered-dolomite was used because of the known difficulties in nucleating ordered-dolomite at 25° C (Berner, 1971, p. 149).

Ca^{2+} and Mg^{2+} concentrations initially increase with a rise in pH and alkalinity, as predicted from weathering (Table 3). This increase is followed by a decrease in concentrations as the pH approaches 10 in samples 7, 9, and 19. Figures 10 and 11 show supersaturation occurs with respect to both calcite and disordered-dolomite when the alkalinity increases above 3 meq. ($10^{0.5}$ meq.). The leveling-off of the activity products with increasing alkalinities is taken as evidence for the precipitation of these phases. Dolomite and calcite are ubiquitous in the Pleistocene sediments, as discussed previously, and their precipitation was to be expected.

A reaction relationship between calcite and disordered-dolomite is important in the formation of sepiolite and kerolite. The reaction is

$$CaMg(CO_3)_{2(s)} + 2H^+ = CaCO_{3(s)} + Mg^{2+} + CO_{2(g)} + H_2O$$

At 25° C and 1 bar the log equilibrium constant for this reaction is 10.16, computed from data given by Helgeson and others (1977). In terms of activities,

$$10.16 = \log a_{Mg^{2+}}/(a_{H^+})^2 + \log f_{CO_2} \quad (1)$$

where a and f are the thermodynamic activity and fugacity, respectively, and unit activities are assumed f on water and solid phases.

A reaction relationship between disordered-dolomite and calcite is shown in the three ground water samples in the vicinity of the massive sepiolite and kerolite deposit. Samples 6, 8, and 18 have log activity products for the above reaction which are nearly identical to the equilibrium value. These are 10.18, 10.17, and 10.22, respectively. The agreement is some-

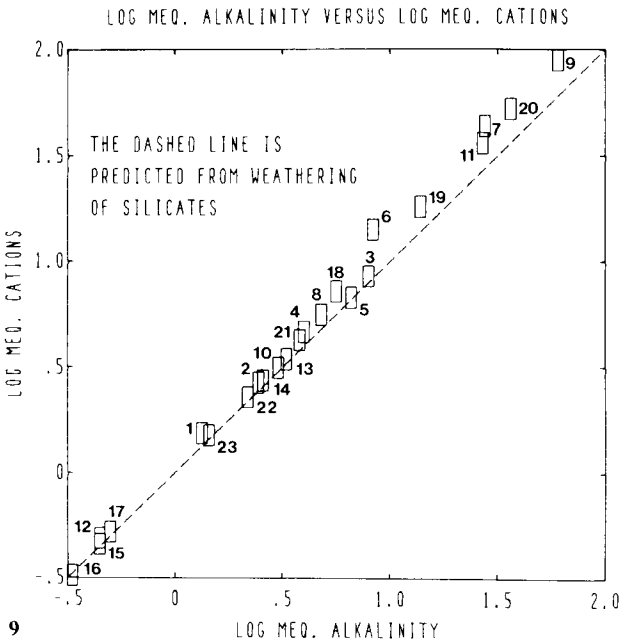

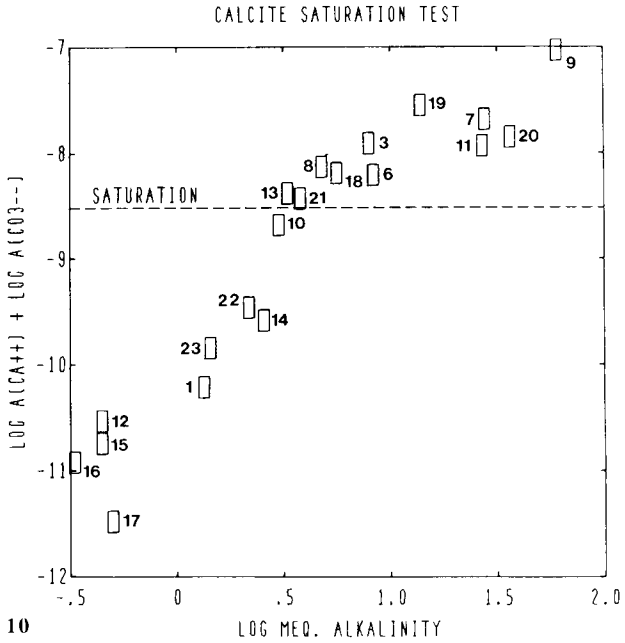

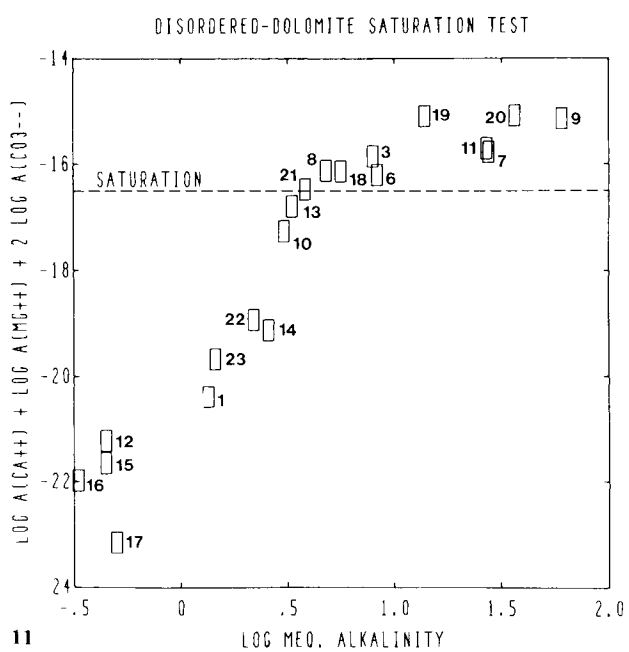

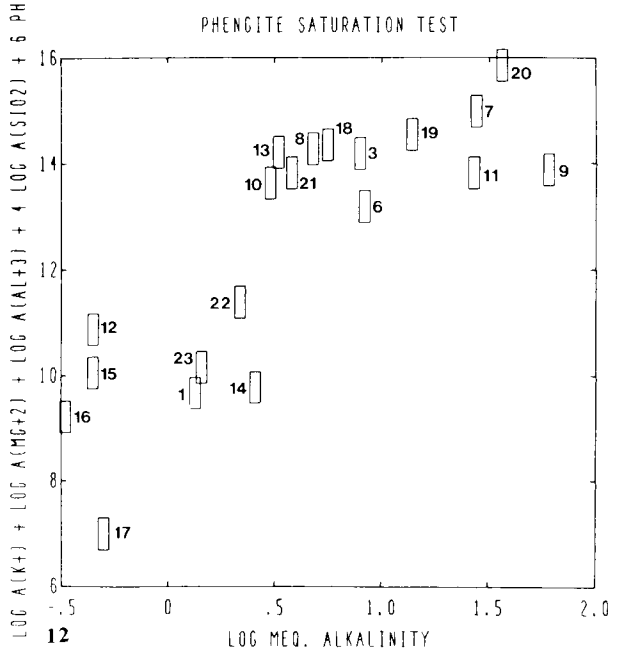

Fig. 9. Log meq. of total cations plotted versus log meq. of alkalinity for Amboseli water samples. Estimated error limits are indicated by the size of the rectangles

Fig. 10. The log activity solubility products for calcite are plotted against the log meq. of alkalinity for Amboseli water samples. The estimated error limits are indicated by the size of the rectangles

Fig. 11. The log activity solubility products for disordered-dolomite are plotted against the log meq. of alkalinity for Amboseli water samples. Estimated error limits are indicated by the size of the rectangles

Fig. 12. The log activity solubility products for a phengite, $KMgAlSi_4O_{10}(OH)_2$, are plotted versus the log meq. of alkalinity for Amboseli water samples. Estimated error limits are indicated by the size of the rectangles

what fortuitous since Figures 10 and 11 show the waters to be slightly supersaturated with respect to both phases. Still, the water chemistries of the three samples in Table 3 show considerable variation; to achieve such consistency in the log activity products almost necessitates a reaction relationship.

Equation (1) buffers the log $a_{Mg^{2+}}/(a_{H^+})^2$ as a function of log f_{CO_2}. In ground waters the variation of log f_{CO_2} is usually between -2 and -3.5; therefore, the log $a_{Mg^{2+}}/(a_{H^+})^2$ will be buffered between 12.2 and 13.7. These limits are delineated on Figure 14, showing that supersaturation with respect to both sepiolite and kerolite will occur in waters having only moderate log a_{SiO_2} values.

With the exception of a low-aluminum, high-magnesium phengite, the activity solubility products of silicates do not level-off with increasing meq. of alkalinity. In general silicate reactions occur too slowly to control the water compositions within the basin. For this reason, Na^+ and K^+ concentrations continue to increase in Table 3 with both increasing alkalinity and pH. These waters in Table 3 are undersaturated with respect to sodium carbonate and bicarbonate phases; therefore, the precipitation of gaylussite, trona, etc. is not reflected in the Na^+ concentration trend.

A low-Al, high-Mg phengite, $KMgAlSi_4O_{10}(OH)_2$, is apparently being precipitated from ground waters in the basin. Figure 12 shows the sample log activity solubility products plotted versus log meq. alkalinity. There is a definite turnover in the log activity solubility product at a value of about 14. We have no thermodynamic data for a phengite of such composition; however, a 25° C and 1 bar standard state free energy of formation of $-1{,}296.8$ kcal mole^{-1} can be computed from the apparent solubility log K of 14 and reference data compiled by Helgeson and Kirkham (1977). The apparent reaction relation shown in Figure 13 may, of course, be fortuitous; however, a 10 Å phase, as discussed earlier, could be kerolite and/or an illite such as a phengite.

The sample data are plotted on 25° C and 1 bar phase diagrams to illustrate trends in the water chemistry (Figs. 13 and 14). Unit activities of solid phases

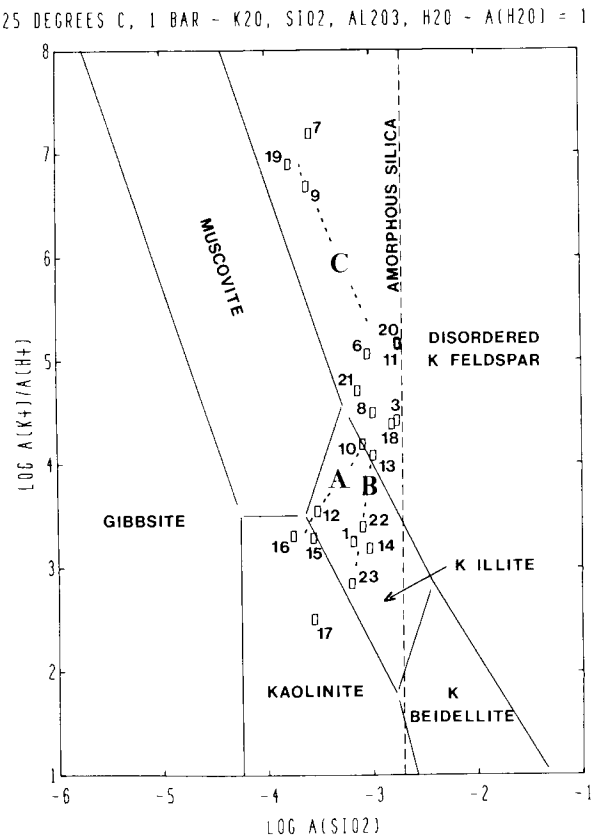

Fig. 13. The log a_K/a_{H^+} plotted versus log a_{SiO_2} for Amboseli water samples. Trends A and B are surface and ground water trends, respectively. Trend C is an evaporation trend. Estimated error limits are indicated by the size of the rectangles

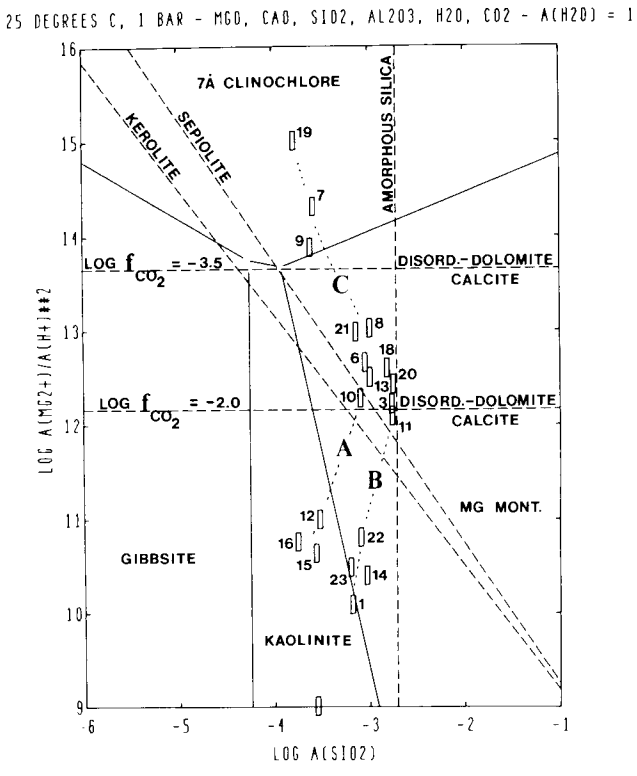

Fig. 14. The log $a_{Mg^{2+}}/(a_{H^+})^2$ plotted versus log a_{SiO_2} for Amboseli water samples. Trends A and B are surface and ground water trends, respectively. Trend C is an evaporation trend. Estimated error limits are indicated by the size of the rectangles

and water are assumed in these diagrams. The mineral stability fields are computed for reactions balanced on aluminum, and the saturation lines are for phases lacking aluminum. Except for the phases discussed below, the standard state free energies of formation of the phases used in the diagrams are from the recent revision of thermodynamic data by Helgeson et al. (1977). Data for sepiolite and kerolite came from Stoessell (1977). The thermodynamic stability of disordered K-feldspar was approximated by sanidine. Data for K illite, K beidellite, and Mg montmorillonite were computed from conventional ideal site mixing models using reference data from Helgeson et al. (1977) and the site occupancies described below.

The standard state free energy of formation of K illite, $K_{0.5}Al_2(Al_{0.5}Si_{0.5})Si_3O_{10}(OH)_2$, was derived by mixing 0.5 moles of pyrophyllite, $Al_2SiSi_3O_{10}(OH)_2$, with 0.5 moles of muscovite, $KAl_2AlSi_3O_{10}(OH)_2$. Similarly, the standard state free energy of formation of K beidellite, $K_{0.33}Al_2(Al_{0.33}Si_{0.67})Si_3O_{10}(OH)_2$, was computed from mixing 0.33 moles of muscovite with 0.67 moles of pyrophyllite. The standard state free energy of formation of Mg montmorillonite, $Mg_{0.165}(Al_{1.67}Mg_{0.33})SiSi_3O_{10}(OH)_2$, was computed by mixing 0.165 moles of talc, $MgMg_2SiSi_3O_{10}(OH)_2$, with 0.835 moles of pyrophyllite. The cations in the formulas above are written in terms of site occupancies; parentheses are used when different cations occupy the same site.

The stability fields of the three clays in Figures 13 and 14 are only meant to be approximate. In reality, even if the methods of estimating the thermodynamic data were absolutely correct, such clays would never form with unit acitivity in nature.

Several trends are shown by dashed lines on Figures 13 and 14. Trends A and B are for dilute surface and ground waters, respectively, and trend C is an evaporation trend. On both diagrams, trends A and B begin in the kaolinite stability field and move towards amorphous silica saturation. A kaolinite precursor, hydrated halloysite, was found in soil samples near the location of water sample 17 (Fig. 1). Figure 14 shows that amorphous silica saturation is reached in the K feldspar stability field; and with increasing concentration, by evaporation, the water compositions move along a path roughly parallel to the stability boundary between K feldspar and muscovite. Authigenic K feldspar is a common phase in the upper Pleistocene sediments at Amboseli.

Trends A and B on Figure 13 show the water compositions becoming supersaturated with respect to both sepiolite and kerolite prior to reaching amorphous silica saturation. The limits of the buffered log $a_{Mg^{2+}}/(a_{H^+})^2$, set by equation (1), are delineated on Figure 14. Sepiolite and kerolite supersaturations are predicted by the buffered log $a_{Mg^{2+}}/(a_{H^+})^2$ and the high SiO_2 concentrations produced by the weathering of basalts. In the absence of aluminum, sepiolite and kerolite would be expected to form, as was the case in the Sinya Beds. In the presence of aluminum, a magnesium aluminum silicate such as the Mg montmorillonite in Figure 14, should form.

Kerolite, as discussed earlier, often appears from field relations to be an alteration product of sepiolite in the massive deposit in the Sinya Beds. The reaction of sepiolite to kerolite is predicted from Figure 14; kerolite is more stable than sepiolite in the normal aqueous solutions found under earth-surface conditions. The alteration may be pH controlled. Siffert (1962) observed he could not nucleate synthetic sepiolite in solutions having a pH below 8. Stoessell (1977) noted, in equilibrium experiments with sepiolite and kerolite, a pH dependency on equilibration of kerolite and sepiolite. His experiments showed equilibration with kerolite occurred in experiments with pH values between 7 and 8, and equilibration with sepiolite occurred in more basic solutions. The ground water samples in the vicinity of the massive sepiolite and kerolite deposit, samples 6, 8, and 18, have pH values ranging from 7.9 to 8.3 (Table 3). Variations in ground water pH may be promoting the alteration of sepiolite to kerolite.

Trend C, the evaporation trend on Figures 13 and 14, shows a decrease in log a_{SiO_2} in the three samples having the highest pH values, samples 7, 9, and 19. This trend is not only due to the formation of the $H_3SiO_4^-$ complex at high pH values but, as shown in Table 3, represents a major decrease in total SiO_2 concentrations. This decrease is thought to result from the overall precipitation of a variety of silicates such as sepiolite, illite, and possibly K feldspar.

The trend in decreasing SiO_2 concentrations at Amboseli began prior to the three samples undergoing evaporative concentrations (samples 7, 9, and 19). Figures 13 and 14 show ground water samples 3, 11, and 20 to be nearly at amorphous silica saturation. These three samples have a pH range of 7.70 to 7.90. Samples 6, 8, 10, 13, 18, and 21 (all ground waters except sample 10) began the trend moving away from amorphous silica saturation and show a pH range of 7.95 to 8.30. Apparently, above a pH of 7.9, silicates begin precipitating at Amboseli. Interestingly, this is approximately the pH minimum of 7.83 which Siffert (1962) found necessary to precipitate magnesium silicates in the laboratory at room temperatures.

The decreasing SiO_2 concentrations shown by trend C on Figures 13 and 14 are a continuation of the ground water trend. It is assumed that with much more evaporative concentration at the locations of samples 7, 9, and 19, these waters would begin

to show an increase in SiO_2 concentrations. Jones et al. (1967) has shown this to be the case for concentrated sodium carbonate and bicarbonate brines in closed basins of volcanic terrain.

Aluminum concentrations were low in all water samples. Apparently, as fast as aluminum is released in weathering reactions, it is precipitated as an aluminum silicate or an aluminum hydroxide.

Conclusions

A massive sepiolite and kerolite deposit occurs in the Sinya Beds. The deposition of the Sinya Beds began with the precipitation of an earlier magnesium silicate. This precipitate is now preserved as sepiolite(?) in the undolomitized cores of nodules within the massive dolomite. The sepiolite could have been precipitated along the spring-fed margins of a lake. Frequent water level fluctuations would have allowed the precipitate to dry and dehydrate, producing the observed desiccation cracks and a nodular texture. Both of these features were later preserved in the dolomitization of the sepiolite.

The massive green sepiolite of the upper Sinya Beds could have been precipitated following a rise in water level. This green sepiolite would lack desiccation cracks because it was not exposed to drying. The absence of nodular texture could be due to dehydration of the precipitate by sediment loading rather than drying in the sun.

The geochemical environment contained very little aluminum. The lack of aluminum may imply that the lake predated the extrusion of the nearby Pleistocene basalts of Kilimanjaro. The chemistry of the mixture of spring and lake waters, producing the sepiolite precipitate, must have included at least moderate Mg^{2+} and SiO_2 concentrations and a pH between 8 and 10. The lower pH limit is inferred from the experiments of Siffert (1962) and those described by Stoessell (1977). The upper pH limit reflects the very low Mg^{2+} concentrations found in CO_3^{2-} and HCO_3^- waters at high pH values (samples 7, 9, and 19 in Table 3).

Ground water dolomitization of the lower sepiolite could have occurred following a shrinking of the lake. Ground waters draining the Precambrian marbles to the north, flowed south through the sepiolite deposit. These waters were probably characterized by a pH between 7 and 8, high concentrations of Ca^{2+} and HCO_3 and low concentrations of Mg^{2+} and SiO_2 (White et al., 1963, p. F22). Such waters would be undersaturated with respect to sepiolite, causing dissolution, and raising the pH and the Mg^{2+} and SiO_2 concentrations. This would produce supersaturation to dolomite and cause precipitation. As the SiO_2 values increased, sepiolite supersaturation occurred, and secondary sepiolite was precipitated in cracks and veins. The process was repeated many times and produced the massive sepiolite within the massive dolomite. The upper extent of dolomitization was marked by the top of the ground water table, producing a relatively sharp transition between the dolomite and the green sepiolite. Kerolite precipitated later either as an alteration product of sepiolite or a direct precipitate in ground water with a pH below 8.

Dolomitization could have ended with the extrusion and near-surface intrusion of the nearby basalts of Kilimanjaro. These tectonic events folded and elevated the Sinya Beds which were then eroded. The ground waters now draining into the Sinya Beds were from Kilimanjaro to the south and had chemical compositions similar to the present ground waters in the area (Table 3). Sepiolite and kerolite could precipitate from these waters in cracks and veins within the massive dolomite and the overlying massive green sepiolite.

The Amboseli Clays were deposited within a lake. Lavas associated with Kilimanjaro could have produced this lake by damming the north-south drainage in the vicinity of the modern lake bed of Lake Amboseli. Williams (1972) postulated such an event; however, he placed it prior to the deposition of the Sinya Beds.

The Amboseli Clays are green lacustrine sediments containing a disseminated, fine-grained mixture of K feldspar, sepiolite, dolomite, calcite, and a 10 Å clay (either illite and/or kerolite). Secondary veins of sepiolite were deposited from ground waters along the bedding planes in the lower Amboseli Clays. The presence of authigenic low temperature K feldspar implies a high salinity within the lake (Hay, 1966, pp. 93–101). The upper Amboseli Clays contain gaylussite indicating an increased salinity during the deposition of these clays.

The lake completely dried up, possibly due to increasing aridity. The lower 01 Tukai Beds, lying above the basal 01 Tukai bed, are primarily composed of clay aggregates of eolian origin. The mineral assemblage could have been derived from erosion and deflation of the underlying Amboseli Clays and the basal bed of the 01 Tukai Beds. Secondary deposits of sepiolite, opaline silica, and calcite fill root casts within the 01 Tukai Beds. The precipitation of these phases is predicted from the present ground water chemistry (Fig. 10 and 14).

The chemistry of the waters within the Amboseli Basin primarily reflects the weathering of the alkaline

olivine basalts. The minerals in the basalts break down easily, producing high concentrations of Mg^{2+} and SiO_2. The waters rapidly become saturated with respect to both sepiolite and kerolite; however, nucleation of these minerals is not rapid enough to maintain equilibrium.

Equilibrium is apparently maintained in the precipitation of calcite and a disordered-dolomite in the area of the Sinya Beds. Equlibrium between calcite and disordered-dolomite buffers the log $a_{Mg^{2+}}/(a_{H^+})^2$ as a function of log f_{CO_2}. This buffering combined with the high SiO_2 concentrations produced from the weathering of basalts, results in a stable supersaturated environment for the precipitation of sepiolite and kerolite (Fig. 14). In the Sinya Beds, the pH varies around the transition pH of 8 which was shown by the experiments of Stoessell (1977) to separate the apparent nucleation of sepiolite from that of kerolite.

Carbonate buffering reactions can be of general importance in explaining the common association of sepiolite and dolomite. The carbonate system supplies both a low-aluminum environment and a buffered log $a_{Mg^{2+}}/(a_{H^+})^2$ as a function of log f_{CO_2}. The lack of aluminum prevents the formation of a smectite or a chlorite. Figure 14 shows that moderate concentrations of SiO_2, produced by weathering silicates outside the carbonate unit, will produce sepiolite supersaturation.

Acknowledgements. Financial support was provided by a Geological Society of America Grant 1991 (1975) to R.K.S., and two National Science Foundation Grants, DES 72-01523 to R.L.H. and DES 74-12782 to Dr. Ian Carmichael. Permission to do field work at Amboseli was granted by the government of Kenya.

We are grateful for the use of field sampling equipment loaned by Dr. R.H. Mariner of the U.S.G.S. at Menlo Park. Laboratory support facilities were supplied by Drs. Ian Carmichael at Berkeley and James Bischoff of the U.S.G.S. at Menlo Park. Richard Reeder performed the microprobe analyses, and Joachim Hampel provided necessary photographic work.

Drs. Ivan Barnes and Blair Jones read an earlier version of the manuscript and offered valuable suggestions. One of us, R.K.S., wishes to acknowledge the scientific input of Philip Behrman, Richard Reeder, and Thure Cerling in many discussions on this project.

References

Bellack, E., Schouboe, P.J.: Rapid photometric determination of fluoride in water. Anal. Chem. **30**, 2032–2034 (1958)

Berner, R.A.: Principles of chemical sedimentology, p. 240. New York: McGraw-Hill 1971

Brindley, G.W.: X-ray and electron diffraction data for sepiolite. Am. Mineralogist **44**, 495–500 (1959)

Brindley, G.W., Bish, D.L., Wan, H.M.: The nature of kerolite, its relation to talc and stevensite. Am. Mineralogist (in press, 1977)

Brown, E., Skougstad, M.W., Fishman, M.J.: Methods for collection and analysis of water samples for dissolved minerals and gases. U.S. Geol. Surv. Techniques of Water-Resources Investigations, Book 5, A1, p. 160 (1970)

Garrels, R.M.: Genesis of some ground waters from igneous rocks. Researches in geochemistry (Abelson, P.H., ed.), Vol. 2, pp. 405–420. New York: Wiley 1967

Garrels, R.M., Christ, C.L.: Solutions, minerals, and equilibria, p. 450. New York: Harper and Row 1965

Hay, R.L.: Zeolites and zeolite reactions in sedimentary rocks. Geol. Soc. Am. Spec. Papers **85**, p. 130 (1966)

Helgeson, H.C.: Thermodynamics of hydrothermal systems at elevated temperatures and pressures. Am. J. Sci. **267**, 729–804 (1969)

Helgeson, H.C., Delany, J.M., Nesbitt, H.W.: Summary and critique of the thermodynamic properties of rock-forming minerals. Am. J. Sci. (in preparation, 1977)

Helgeson, H.C., Kirkham, D.H.: Theoretical prediction of the thermodynamic behavior of aqueous electrolytes at high pressures and temperatures. IV. Calculation of activity coefficients, osmotic coefficients, and apparent molal and standard and relative partial molal properties to 5 kb, 600° C, and >6 m. Am. J. Sci. (in preparation, 1977)

Jones, B.F., Rettig, S.L., Eugster, H.P.: Silica in alkaline brines. Science **158**, 1310–1314 (1967)

Kharaka, Y.F., Barnes, I.B.: *Solmneq*: solution-mineral equilibrium computations. U.S. Dept. Commerce, *PB-215* **899**, p. 82 (1973)

Maksimović, Z.: β-kerolite-pimelite series from Goleš Mountain Yugoslavia. Proc. Internat. Clay Conf., Jerusalem, Israel **1**, 97–105 (1966)

Martin, R.F.: Disordered authigenic feldspars. Am. J. Sci. **56**, 281–291 (1971)

Papke, K.G.: A sepiolite-rich playa deposit in southern Nevada. Clay Minerals **20**, 211–215 (1972)

Parry, W.T., Reeves, C.C., Jr.: Sepiolite from pluvial Mound Lake, Lynn and Terry Counties, Texas. Am. Mineralogist **53**, 984–993 (1968)

Reed, M.: Geologic and geochemical environment of deposition of the massive copper-iron-sulfide ore deposits, West Shasta District, California. Ph. D. thesis, Univ. of California, Berkeley (1977)

Rogers, L.E.R., Quirk, J.P., Norrish, K.: Occurrence of an aluminum-sepiolite in a soil having unusual water relationships. J. Soil Sci. **7**, 177–184 (1956)

Sampson, D.N.: Sinya meerschaum mine, northern Tanzania. Inst. Min. Met. Trans. **75**, B23–B34 (1966)

Shapiro, L., Brannock, W.W.: Rapid analysis of silicate, carbonate, phosphate rocks. U.S. Geol. Surv. Bull. *1144-A*, p. 55 (1962)

Siebert, R.M.: The stability of $MgHCO_3^+$ and $MgCO_3$ from 10° C to 90° C. Ph. D. thesis, Univ. of Missouri, Columbia (1974)

Siffert, B.: Some reactions of silica in solution: formation of clay. Reports Geol. Map Service Alsace-Lorraine **21**, p. 100 (1962)

Stoessell, R.K.: Geochemical studies of two magnesium silicates, sepiolite and kerolite. Ph. D. thesis, Univ. of California, Berkely (1977)

Stumm, W., Morgan, J.J.: Aquatic chemistry, p. 583. New York: John Wiley 1970

Tabatabai, M.A.: Determination of sulphate in water samples. Sulphur Inst. J. **10**, No. 2, p. 3 (1974)

White, D.E., Hem, J.D., Waring, G.A.: Chemical composition of subsurface waters. U.S. Geol. Surv. Profess. Papers *440-F*, p. 67 (1963)

Williams, L.A.J.: Geology of the Amboseli area. Geol. Surv. Kenya **90**, p. 86 (1972)

Received May 6, 1977 / Accepted September 30, 1977